AGU PUBLICATIONS

JGR

Journal of Geophysical Research: Space Physics

RESEARCH ARTICLE
10.1002/2014JA020426

Special Section:
Origins and Properties of Kappa Distributions

Key Points:
- Particles accelerated in the heliosphere have a common spectrum
- Traditional acceleration mechanisms do not yield the common spectrum
- A pump acceleration mechanism does yield the common spectrum

Correspondence to:
L. A. Fisk,
lafisk@umich.edu

Citation:
Fisk, L. A., and G. Gloeckler (2014), The case for a common spectrum of particles accelerated in the heliosphere: Observations and theory, *J. Geophys. Res. Space Physics*, *119*, 8733–8749, doi:10.1002/2014JA020426.

Received 23 JUL 2014
Accepted 21 OCT 2014
Accepted article online 25 OCT 2014
Published online 19 NOV 2014

The case for a common spectrum of particles accelerated in the heliosphere: Observations and theory

L. A. Fisk[1] and G. Gloeckler[1]

[1]Department of Atmospheric, Oceanic and Space Sciences, University of Michigan, Ann Arbor, Michigan, USA

Abstract In the last decade a significant discovery has been made in the heliosphere: the spectrum of particles accelerated in both the inner heliosphere and in the heliosheath is the same: a power law in particle speed with a spectral index of −5, when the spectrum is expressed as a distribution function; or equivalently, a differential intensity spectrum that is a power law in energy with a spectral index of −1.5. In the inner heliosphere this common spectrum occurs at quite low energies and is most evident in instruments designed to measure suprathermal particles. In the heliosheath, the common spectrum is observed over the full energy range of the Voyager energetic particle instruments, up to energies of ~100 MeV. The remarkable discovery of a common spectrum is compounded by the realization that no traditional acceleration mechanism, i.e., diffusive shock acceleration or stochastic acceleration, can account for the common spectrum. There is thus an opportunity to once again demonstrate the relevance of heliospheric physics by developing a new acceleration mechanism that yields the common spectrum, with the expectation that such a new acceleration mechanism will find broader applications in astrophysics. In this paper, the observations of the common spectrum in the heliosphere are summarized, with emphasis on those that best reveal the conditions in which the acceleration must operate. Then, building on earlier work, a complete derivation is presented of an acceleration mechanism, a pump acceleration mechanism, that yields the common spectrum, and the various subtleties associated with this derivation are discussed.

1. Introduction

In the last decade, detailed observations have been made of the spectra of lower energy particles accelerated both in the inner heliosphere, from the Ulysses and ACE spacecraft, and in the heliosheath beyond the termination shock of the solar wind, from the Voyager spacecraft. In both cases, in specific events in the inner heliosphere, and throughout the heliosheath, the spectra are the same: a power law in particle speed with a spectral index of −5, when the spectrum is expressed as a distribution function (also referred to as phase space density); or equivalently, a differential intensity spectrum that is a power law in energy with a spectral index of −1.5. This common spectrum generally has an exponential rollover at higher energies, indicating the maximum energy particles acquire in the acceleration process.

In the inner heliosphere the common spectrum occurs at quite low energies, in all cases less than ~1 MeV/nucleon, and in many cases below ~100 keV/nucleon, which makes it most evident in the observations of the Solar Wind Ion Composition Spectrometer (SWICS) instruments on ACE and Ulysses [*Gloeckler et al.*, 1992]; these observations are summarized in *Fisk and Gloeckler* [2012a]. In the heliosheath, the common spectrum is observed over the full energy range of the Voyager Low-Energy Charged Particle Experiment and Cosmic Ray Subsystem instruments [*Krimigis et al.*, 1997; *Stone et al.*, 1977]. Shortly after both Voyagers 1 and 2 crossed the termination shock, the common spectrum (an intensity spectrum with spectral index of −1.5) was observed in particles accelerated to about a few MeV/nucleon [*Decker et al.*, 2006; *Gloeckler et al.*, 2008]. Not only was the spectral index the same at both Voyagers 1 and 2 but also the absolute intensity was the same at both spacecraft, even through the two Voyagers were more than 100 AU apart, and these common spectra remained essentially unchanged for years after the termination shock crossings. Moreover, when Voyager 1 reached the prime acceleration region of the anomalous cosmic rays (ACRs) at ~117 AU, the full ACR oxygen spectrum had the common spectrum [*Fisk and Gloeckler*, 2013, and references therein].

It is remarkable that the spectra of accelerated particles in the inner heliosphere and in the heliosheath are the same. It is also remarkable that no traditional acceleration mechanism, such as diffusive shock

acceleration or stochastic acceleration, can account for the common spectrum. Diffusive shock acceleration does yield power law spectra, but in general the spectral index depends on the compression ratio of the shock, with no preference for a spectral index of −5. Traditional stochastic acceleration often yields exponential spectra, and if power laws result, there is again no reason for a spectral index of −5.

We have then a new discovery in heliospheric physics—the common spectrum—and the need for a new acceleration mechanism to explain the common spectrum. We should also have the expectation that the new acceleration mechanism will find broad application to other astrophysical settings, which is after all one of the strengths of heliospheric physics; we have the opportunity to study new phenomena in detail that can be applied broadly to astrophysics and particles accelerated in the solar corona. There is a need, then, for a concerted theoretical effort to both explain the common spectrum and, by using the extensive observations that are available, to validate the explanations that are developed.

In a series of papers, *Fisk and Gloeckler* [2007, 2008, 2012a] and *Fisk et al*. [2010] developed a new acceleration mechanism that yields the common spectrum, a pump mechanism that accelerates particles in compressive turbulence in regions of space that can be considered to be thermally isolated, i.e., no external sources of energy. We will discuss the pump acceleration mechanism in detail in this paper and show that it can account for the observations. The concept that the common spectrum results from acceleration of a low-energy source of particles in compressive turbulence, in a thermally isolated volume, is supported by earlier theoretical work by *Bykov* [2001], who found the common spectrum in superbubbles before the common spectrum was known in the heliosphere. *Bykov* [2001] performed a nonlinear numerical simulation, in which there is a reaction of the accelerated particles on the turbulence, such that energy is conserved between the accelerated particles and the turbulence. The requirement that energy is conserved is equivalent to the requirement in the work of Fisk and Gloeckler that the acceleration occurs in a thermally isolated system, with no external source of energy. With this requirement, the acceleration is not a traditional stochastic acceleration, since now the acceleration process has a coupling between different particle components, and is no longer a Markov process. The resulting nonrelativistic distribution function of the accelerated particles found by *Bykov* [2001] is a power law with a spectral index of −5.

Jokipii and Lee [2010] were content with criticizing the theory of Fisk and Gloeckler but offered no explanation of their own for the common spectrum. *Schwadron et al*. [2010] provided a statistical argument for the common spectrum, which is readily incorporated into the pump acceleration mechanism, as discussed in *Fisk et al*. [2010]. *Livadiotis and McComas* [2009, 2011, 2012, 2013] have approached this problem through the application of nonequilibrium thermodynamics, Tsallis statistical mechanics, and the application of kappa functions. *Zhang and Lee* [2013] followed an approach similar to *Bykov* [2001] by arguing that the common spectrum, with spectral index of −5, could result from a back reaction of the accelerated particles on the turbulence, thus limiting the energy in the accelerated particles. However, no details were provided as to how this process would work or were there any comparisons with observations. *Antecki et al*. [2013] argued that the limiting process that maintains finite energy in the accelerated particles, and thus limits the spectrum to −5, could be adiabatic deceleration in the solar wind. However, as we discuss in this paper, the −5 spectrum develops quickly immediately downstream from shocks, where adiabatic deceleration is unlikely to be important. Drake and coworkers [e.g., *Drake et al*., 2013] have shown that a −5 spectrum can result from particles being accelerated by interacting with magnetic islands that result from the extensive reconnection they expect in the heliosheath. This mechanism cannot explain acceleration in the inner heliosphere, where although reconnection is observed in the solar wind, there is no evidence to suggest any substantial nonthermal particle acceleration [e.g., *Gosling*, 2012].

In this paper, we first summarize the observations of the common spectrum in the heliosphere, emphasizing those observations that best reveal the conditions in which the acceleration must operate. We then build upon the earlier work of *Fisk et al*. [2010] and *Fisk and Gloeckler* [2012a] and provide a complete derivation of a pump acceleration mechanism that yields the common spectrum, discussing the various subtleties associated with this derivation. In section 4, we comment on the applications of the pump acceleration mechanism that have been developed to date, including applying it to the acceleration of galactic cosmic rays in the galaxy, as well as on other possible applications that are currently underway, such as the acceleration of solar energetic particles.

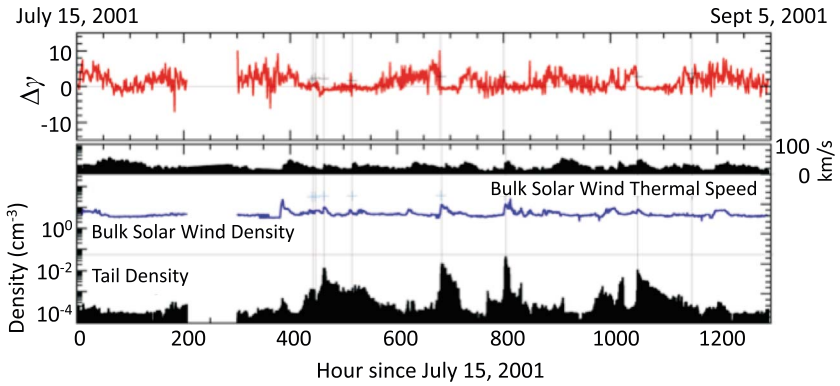

Figure 1. Variations with time during a CME-dominated 54 day period of (top) deviation from 1 of the ratio of hourly values of the power law spectral indices of the proton low-tail ($V_{sw} < v_{proton} < 3V_{sw}$) to high-tail ($3V_{sw} < v_{proton} < 9V_{sw}$) segments and (bottom) hourly values of the bulk solar wind thermal speed, V_{th}, solar wind density, and the density of tail particles ($V_{sw} < v_{proton} < 9V_{sw}$). In the solar wind frame, v_{proton} is the speed of protons. Eight shocks were recorded during this 54 day period at times indicated by the vertical lines.

2. The Key Observations of the Common Spectrum

The best and arguable only way to obtain definitive information on where particles are accelerated, and the acceleration mechanism responsible, is through observations of differential intensity spectra or velocity distributions of (a) several species with different charge-to-mass (Q/A) ratios (b) over a broad energy range (from $<$1 keV/nucleon to $>$100 MeV/nucleon) in the location where the particles are accelerated.

In the inner heliosphere, there are instances of substantial enhancement of particle intensities, over a wide energy range, typically below a few MeV, lasting from hours to days. We refer to these events as Local Acceleration Events (LAEs) and the location in which they occur as Local Acceleration Regions (LARs). This nomenclature does not prejudice the acceleration process responsible for the LAEs, since, as we shall discuss, sometimes the LAEs are accompanied by locally recorded shocks (e.g., energetic solar particle (ESP) events and co-rotating interaction region (CIR)); however, the main acceleration is generally not coincident with a shock. Beyond the termination shock, the entire nose region of the heliosheath can be considered to be a large local acceleration region (LAR).

Within the LARs there often are embedded prime acceleration regions (PARs) in which particle intensities are at local maximum values. In these PARs, contributions from remote acceleration regions are small. There, the operating acceleration mechanism produces energy spectra that are not contaminated by particles accelerated remotely.

In this section we present observations that best reveal the conditions in which the acceleration of the common spectrum must occur: (1) spectra of particles (mostly protons) accelerated downstream from shocks in the slow wind at 1 AU, (2) the acceleration of ACRs in the heliosheath, and (3) acceleration in the fast solar wind from the polar coronal holes. All of the spectra that we will show have been transformed to the solar wind frame using the duty cycle approximation. It is essential to make this transformation to the solar wind frame to observe the true spectral shapes, especially in the SWICS energy range, below ~100 keV/nucleon.

With knowledge of the required conditions in which the acceleration of the common spectrum must occur, we can develop an acceleration mechanism that can yield the common spectrum, in the next section.

2.1. The Common Spectrum in the Inner Heliosphere

In Figure 1 we show the variations with time of the hourly values of the density of suprathermal tails observed with SWICS on ACE during a 54 day period in 2001, computed by integrating the solar wind frame distribution function of protons from $v_{proton} = V_{sw}$ (the solar wind speed) to $v_{proton} = 9V_{sw}$. The tail density is highly variable, from low values of ~$5 \cdot 10^{-5}$ cm^{-3} to values exceeding 10^{-2} cm^{-3}. Local peak tail densities are often (but not always) associated with shocks. However, half of the shocks produce no local peaks, and several local peaks are not accompanied by shocks. This result is consistent with the results of a statistical study of numerous shocks and ESP events by *Lario et al.* [2005].

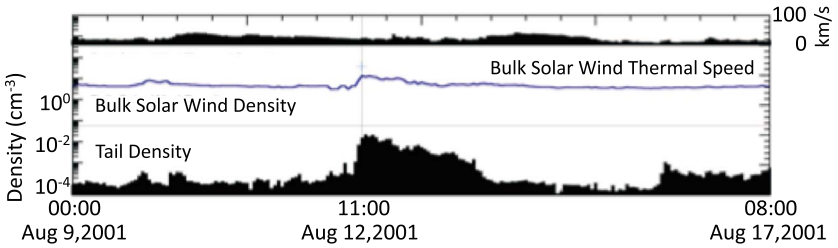

Figure 2. Same as Figure 1 (bottom) but now on an expanded timescale.

In Figure 1 (top) are plotted the hourly values of $\Delta\gamma$ representing the difference between the best fits of the power law index of the lower-speed portion of the tail and the higher-speed portion. When $\Delta\gamma = 0$ the indices are the same. In general $\Delta\gamma$s are highly variable and not equal to zero, i.e., for much of the time pure power law spectra are not observed. However, in LAEs, downstream of shocks, variations in $\Delta\gamma$ become small; its value is zero, and, as we will show later, the power law index of the entire tail is then -5.

2.1.1. The 12 August 2001 Local Acceleration Event

We select the second of the most intense of the four LAEs shown in Figure 1. It was accompanied by a strong shock ($r_{comp} = 3.85 \pm 0.05$, $V_{sh} = 409 \pm 29$ km/s, $\theta_{Bn} = 76 \pm 3°$, and $M_A = 2.8$), observed by the magnetometer and the Solar Wind Electron, Proton, and Alpha Monitor on ACE on 12 August 2001 at 10:50. The time profiles of the solar wind thermal speed and of the densities of the solar wind and tail are displayed in Figure 2. While the solar wind density ramped up over several hours to reach a peak at the shock, the thermal speed showed only a modest increase at the shock. The tail density (protons with speeds between V_{sw} and $9V_{sw}$) ramped up from a low value of $\sim 3 \cdot 10^{-4}$ cm^{-3} to $\sim 1.5 \cdot 10^{-2}$ cm^{-3} at the shock, reaching its peak value of $\sim 2.5 \cdot 10^{-2}$ cm^{-3} 1 h downstream of the shock.

In Figure 3 (left) we show the 1 h averaged proton spectrum during the hour of shock passage at ACE. The solar wind frame velocity distribution shows the bulk solar wind (assumed to be Maxwellian), a halo component ($3V_{th} < v_{proton} < V_{sw}$) that could be fit by a kappa function, and the tail component ($v_{proton} > V_{sw}$). A close examination of the tail spectrum reveals it to be a -5 power law above $v_{proton} \approx 2.5V_{sw}$. Below that speed and up to the end of the halo, the spectrum bends down. This bend down suggests that the observed tail spectrum at the shock is a modulated spectrum of particles accelerated not at the shock itself but most likely further downstream of the shock. Indeed, the 1 h averaged solar wind-frame proton spectrum taken at the peak of the tail density, 1 h downstream of the shock (Figure 3, right), shows a perfect -5 power law tail from ~400 to >3000 km/s.

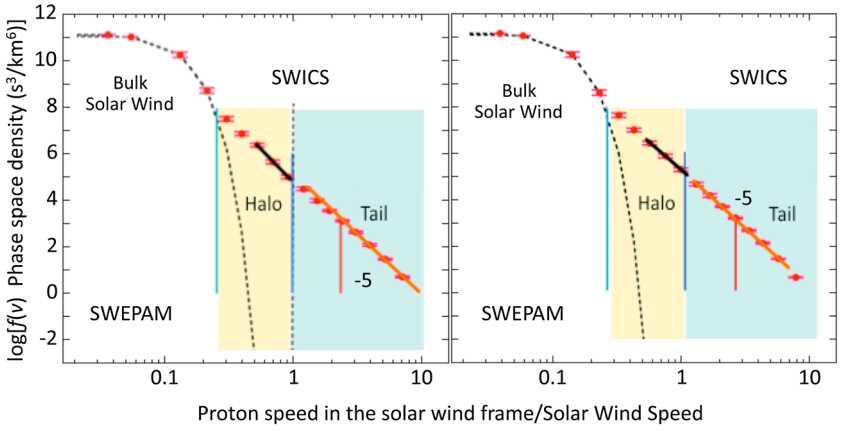

Figure 3. One-hour averaged solar wind frame velocity distribution functions showing the proton bulk solar wind, the halo, and the tail segments during hour 11 of 12 August 2001, (left) during which the strong (compression ratio of 3.85 ± 0.15) shock passed ACE and (right) during the hour of peak tail density that was observed 1 h downstream of the shock.

Table 1. Parameters Characterizing the Tail Spectra at the Shock and at the Peak Tail Density for Major LAEs Observed in August 2001

Date of LAE	Averaging Interval	Location	Comp. Ratio r	θ_{Bn}	γ	v_{high} (cm/s)[c]	v_{low} (cm/s)
17 Aug 2001	10:00–11:00	shock	4.3 ± 0.9	$62° \pm 6°$	5.07 ± 0.09	$>3.5 \cdot 10^8$	$\sim 5 \cdot 10^6$
17 Aug 2001	12:00–14:00	peak	——	——	4.98 ± 0.06	$\sim 3 \cdot 10^8$	0
12 Aug 2001	11:00–12:00	shock	3.85 ± 0.9	$76° \pm 3°$	5.00 ± 0.08	$>3.5 \cdot 10^8$	$5 \cdot 10^7$
12 Aug 2001	12:00–13:00	peak	——	——	5.04 ± 0.06	$\sim 3 \cdot 10^8$	0
3 Aug 2001	06:00–07:00	shock	2.9 ± 0.7	$70° \pm 3°$	5.07 ± 0.10	$2 \cdot 10^8$	$\sim 5 \cdot 10^6$
3 Aug 2001	08:00–09:00	peak	——	——	5.03 ± 0.09	$2 \cdot 10^8$	0
27 Aug 2001	20:00–21:00	shock	2.8 ± 0.6	$89° \pm 6°$	4.99 ± 0.08	$>3.5 \cdot 10^8$	$\sim 10^6$
27 Aug 2001	21:00–02:00[a]	peak	——	——	5.03 ± 0.09	$2 \cdot 10^8$	0
24 Aug 2001	07:00–22:00[b]	diffuse[c]	——	——	4.99 ± 0.09	$>3.5 \cdot 10^8$	0
26 Aug 2001	05:00–18:00	prompt[d]	——	——	4.94 ± 0.07	$2 \cdot 10^8$	0

[a] 28 Aug 2001.
[b] 25 Aug 2001.
[c] Hour 960 of Figure 1.
[d] Hour 1008 of Figure 1.

The tail spectra were fit using equation (1)

$$f(v) = f_0 \left(\frac{v}{10^{7.5}} \right)^{-\gamma} \exp\left(-\frac{v_{low}}{v} \right) \exp\left(-\frac{v}{v_{high}} \right). \quad (1)$$

Here v is the proton speed in the solar wind frame, v_{low} is the e-folding speed for the turndown due to propagation, and v_{high} the e-folding rollover speed.

The results for the 12 August 2001 LAE and five other LAEs in August 2001 are given in Table 1. The most striking result is that during the peak tail density of each LAE a pure -5 power law is observed, in most cases from the end of the bulk solar wind segment ($v_{proton} \approx 3V_{th}$) to the end of the SWICS energy range. The tail spectra at the four shocks with compression ratios ranging from ~2.5 to 4 were modulated -5 power law spectra of particles accelerated downstream of the shocks.

It should be noted that diffusive shock acceleration applied to realistic shocks, which have, for example, nonplanar shock geometries and time variations, can yield complex spectra at the shock front and downstream. However, diffusive shock acceleration will not result in a -5 power law tail that peaks downstream from shocks, as is observed. Thus, the most reasonable explanation for the complex spectra seen at the shock front is that they are the modulated spectra of the particles accelerated downstream.

2.1.2. The 25 October 2001 Local Acceleration Event

Associated with the so-called Halloween events was the large LAE shown in Figure 4. Plotted as a function of time is the 12 min and sector-averaged proton phase space densities of the bulk solar wind ($v_{proton} < 3V_{th}$), the halo ($3V_{th} < v_{proton} < V_{SW}$), the low-speed portion of the tail ($V_{SW} < v_{proton} < 3V_{SW}$), and the high-speed portion of the tail ($3V_{SW} < v_{proton} < 9V_{SW}$). Also shown on the top of the figure is the relationship of the various features of these profiles to the passage past ACE of the LAR, most likely an interplanetary coronal mass ejection (ICME). We envision the LAR to be a 3-D region in space moving away from the Sun at the speed (~400 to 450 km/s in the present case) of the strong shock at its nose. Compared to its surroundings, the LAR is a region of enhanced solar wind density and high compressive turbulence. The density and turbulence levels are by no means uniform throughout the LAR. Rather, there are "hot" spots (red regions) where the solar wind density and turbulence reach their highest levels. These hot spots are the prime acceleration regions (PARs) where the intensities of locally accelerated particles are so high that contributions from remotely accelerated particles are unimportant.

In the frame of the LAR, ACE moved to the right, as indicted (for simplicity) by the dashed line. The strong shock ($r_{comp} \approx 4$, $M_A \approx 3.6$, $\theta_{Bn} = 30° \pm 22°$) passed ACE at 8:01 on 25 October 2001 (see Figure 4, bottom). About half an hour downstream of the shock, ACE entered the first PAR, leaving it ~3 h later. Then, about 24 h after shock passage, ACE entered a second PAR and spent the next 11 h in it.

The sector-averaged solar wind frame phase space densities as a function of w (the ratio of v to the solar wind flow speed) of H^+, He^{++}, He^+, and ^4He averaged over a 12 min time period for the 25 October 2001 LAE are shown in Figure 5. The spectra recorded at shock passage (Figure 5, left) are complex and

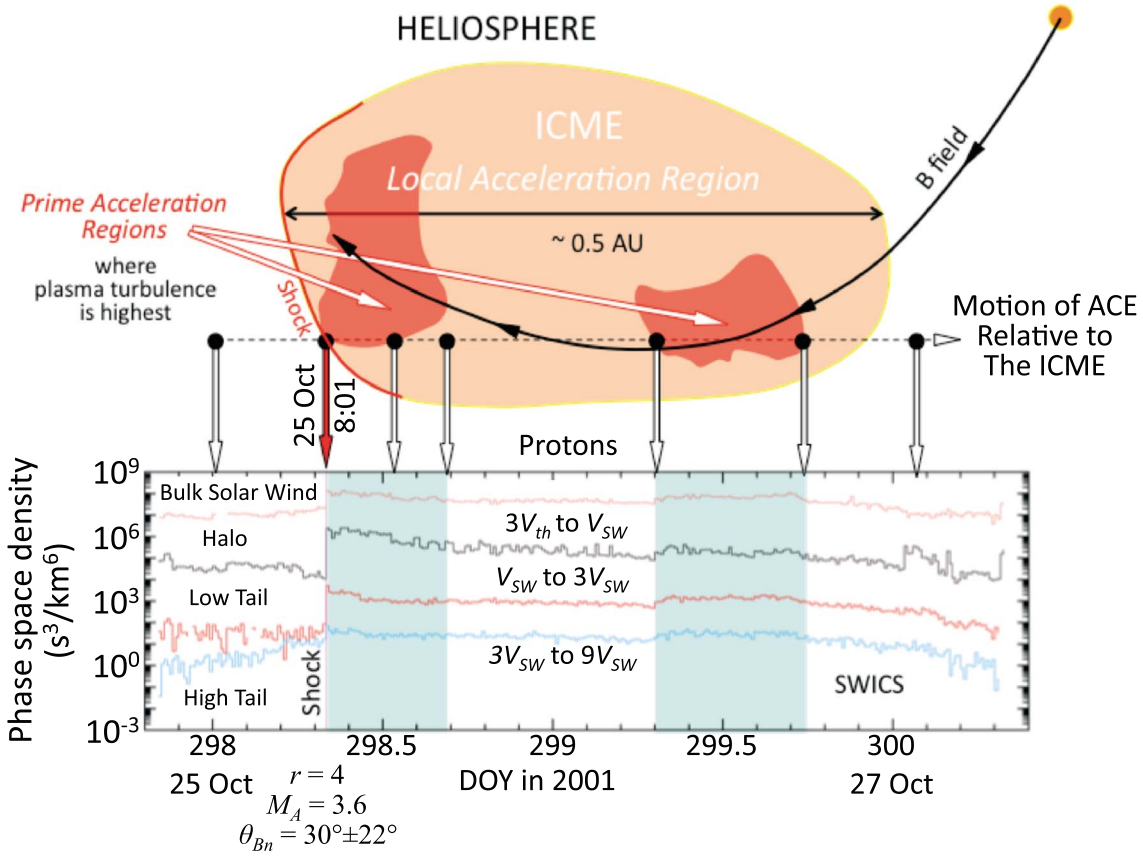

Figure 4. Cross-sectional view of the (top) Local Acceleration Region that produced the 25 October 2001 LAE. (bottom) Time profiles of 12 min and sector-averaged proton phase space densities of the bulk solar wind ($v_{proton} < 3V_{th}$), the halo ($3V_{th} < v_{proton} < V_{SW}$), the low-speed portion of the tail ($V_{SW} < v_{proton} < 3V_{SW}$), and the high-speed portion ($3V_{SW} < v_{proton} < 9V_{SW}$).

multicomponent. There are modulated, high-density spectra of H and ^{4}He above w of approximately 2, and lower density but still prominent halo components. He^+ has the standard pickup He spectrum with a broad rollover at $w \approx 1$ and no measured fluxes above $w \approx 2$, i.e., due to poor statistics no He^+ counts were recorded in the 12 min average.

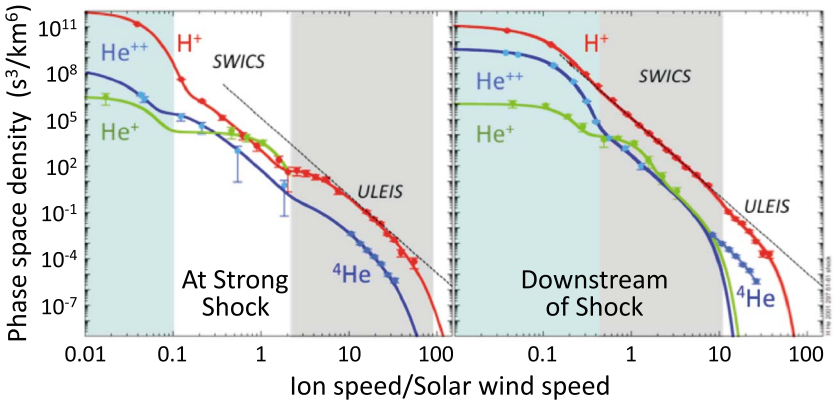

Figure 5. Twelve-minute and sector-averaged solar wind frame velocity distribution functions of H^+, He^{++}, He^+, and ^{4}He measured during the (left) 12 min interval of shock passage (25 Oct 2001 8:01) and (right) ~25 min downstream of the shock. The dotted lines are −5 power laws.

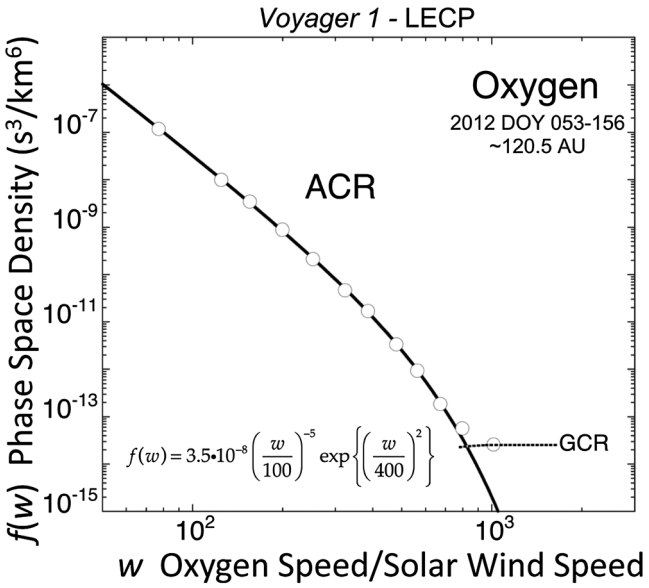

Figure 6. Phase space density of ACR oxygen as a function of oxygen speed/solar wind in the prime acceleration region at ~120 AU. The solar wind speed is taken to be 100 km/s. The equation shown in the figure is the formula for the common spectrum and provides an excellent fit to the observations.

In contrast to this, the 12 min averaged spectra taken about half an hour after shock passage, with ACE in the front section of the first PAR, are −5 power law tails with rather sharp rollovers at $w < \sim 10$. (The sharp rollover for H can be inferred from its spectral shape, the rollovers for He^{+} and He^{++} cannot be determined in these spectra due to poor statistics). For speeds above $w \approx 10$ one observes modulated, lower density spectra with rollovers at $w \approx 25$.

It is important to emphasize that the observations presented in this section show that the role of shocks, even of a strong, quasi-parallel shock (e.g., 25 October 2001) in accelerating particles (i.e., producing strong tails), is minimal. The acceleration is shown to take place in Local Prime Acceleration Regions removed from the shocks. There, the observed high-density spectra, in all cases we have examined so far, are the common spectrum: −5 power law tails with rollovers at characteristic speeds in the w range of 7 to 10. These tails often begin at particle speeds of several times that of the bulk solar wind flow speed.

2.2. The Common Spectrum of ACRs Accelerated in the Nose of the Heliosheath

The Voyager spacecraft are currently exploring the nose region of the heliosheath and find it to be a region of extensive particle acceleration, in effect one large Local Acceleration Region. Unlike LARs in the inner heliosphere that are in motion and whose size, shape, and properties may change rapidly as they travel away from the Sun, the nose of the heliosheath is a stationary region of approximately constant size and shape, extending from the termination shock whose distance from the Sun, typically 80 to 100 AU, is controlled by the supersonic solar wind, to the heliopause, some 40 AU beyond the termination shock [*Fisk and Gloeckler*, 2014; *Gloeckler and Fisk*, 2014]. The solar wind moves through the stationary heliosheath with a constantly diminishing radial speed that at ~115 AU (Voyager 1) reaches its lowest value of only about a km/s and continues at this speed until it reaches the heliopause. The pickup ions produced inside the termination shock are heated by the termination shock and become the dominant pressure in the immediate downstream region of the termination shock. The magnetic field is mostly azimuthal in the nose of the heliosheath and exhibits regions with strong compressions and expansions.

Within a short distance downstream from the termination shock, both Voyagers 1 and 2 observed the common spectrum (an intensity spectrum with spectral index of −1.5) for particles accelerated to about a few MeV/nucleon [*Decker et al*., 2006; *Gloeckler et al*., 2008]. The termination shock thus behaves as do shocks in the inner heliosphere discussed in section 2.1. The common spectrum is not observed at the shock but rather downstream. Moreover, the common spectrum seen by Voyagers 1 and 2 had the same absolute intensity, even through the two Voyagers were more than 100 AU apart, and these common spectra remained essentially unchanged for years after the termination shock crossings.

Further into the heliosheath, the Voyager 1 observations of *Stone et al*. [2013] and *Krimigis et al*. [2013] reveal that ACRs, which are accelerated out of the pickup ions, attain their highest energies at ~117 AU. This is then the prime acceleration region for ACRs. Shown in Figure 6 is the ACR O spectrum observed by *Krimigis et al*. [2013] in the PAR for ACRs. The spectrum is well fit by the common spectrum, an intensity spectrum that is a power law with spectral index of −1.5, with an exponential cutoff at ~100 Mev.

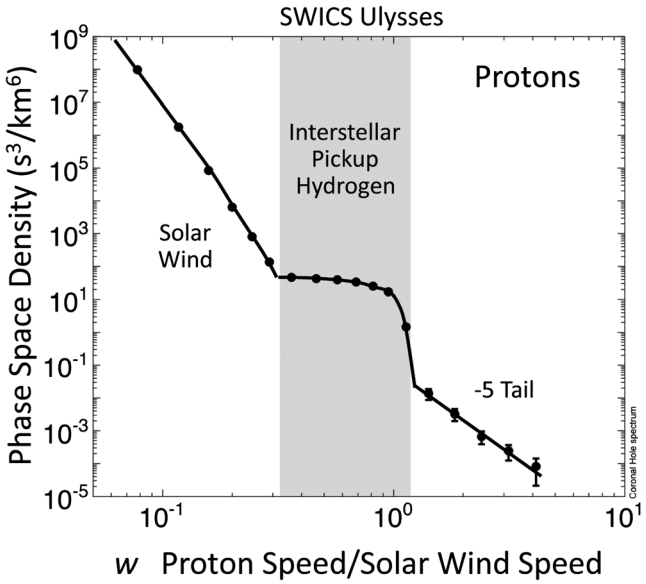

Figure 7. Phase space density of protons versus v_{proton}, the proton speed in the solar wind frame divided by the average solar wind speed measured by Ulysses-SWICS in the fast high-latitude solar wind from the large polar coronal holes. Data from the southern and northern polar passes were combined in order to improve counting statistics at the highest energies of SWICS.

As is discussed in detail in *Fisk and Gloeckler* [2013], the acceleration of the ACRs must be in the heliosheath and cannot occur at the termination shock. The pressure in the ACRs in the PAR is observed to be about half the total particle pressure in the heliosheath [*Gloeckler and Fisk*, 2010]. If ACRs originate at the termination shock on the flanks, as suggested by *Schwadron and McComas* [2006], the ACR pressure would be added to the pressure in the pickup ions that are convected radially downstream from the termination shock with the solar wind. Pressure would then not be constant, as is required in the subsonic heliosheath, unless the pickup ion pressure could be reduced, which seems unlikely. Rather, it is necessary to accelerate the ACRs out of the pickup ions in the PAR.

2.3. The Common Spectrum in the Fast, Polar Coronal Holes Solar Wind

Ulysses pioneered the exploration of the high-latitude heliosphere. During solar minimum it studied the properties of the fast solar wind emanating from the large polar coronal holes. This solar wind was found to be remarkably quiet, with no shocks or Local Acceleration Events recorded during the high-latitude passes at or near solar minimum.

Using data from the SWICS instrument on Ulysses it is possible to characterize the proton velocity distribution in the fast solar wind both in the Northern and Southern coronal holes. The proton spectrum, combining data from the southern and northern high-latitude passes around solar minimum, is shown in Figure 7. One of the most interesting features of this spectrum is the discovery of a suprathermal tail. These were months and months of superquiet times, no shocks, and no LAEs. Yet not only is there a tail but also this tail is the common spectrum. The tail, however, is very weak compared to the tails discussed in section 2.1, for acceleration in the slow solar wind. At $v_{proton} \approx 5 \cdot 10^7$ cm/s the extrapolated phase space density is only $f_0 \approx 0.5\ s^3/km^6$.

3. An Acceleration Mechanism That Yields the Common Spectrum

In this section we develop an acceleration mechanism that yields the common spectrum and derive an equation that describes the time evolution of the common spectrum. We begin by specifying the conditions in which the acceleration mechanism must operate, as revealed by the observations discussed in section 2. We then describe an acceleration mechanism that will accelerate particles under these conditions and yield the common spectrum. We present a derivation of the equation that governs this acceleration and discuss the subtleties and implications of both the derivation and the governing equation. It is this governing equation that can be used to fit observations of the common spectrum, in whatever astrophysical setting it occurs.

3.1. The Conditions in Which the Acceleration Must Operate

As discussed in section 2.2, the most pronounced common spectrum is the ACR spectrum in the heliosheath, which is a subsonic region, with extensive and relatively large-scale compressions and expansions of the solar wind. There is also a ready source of particles to accelerate—the interstellar pickup ions. The common

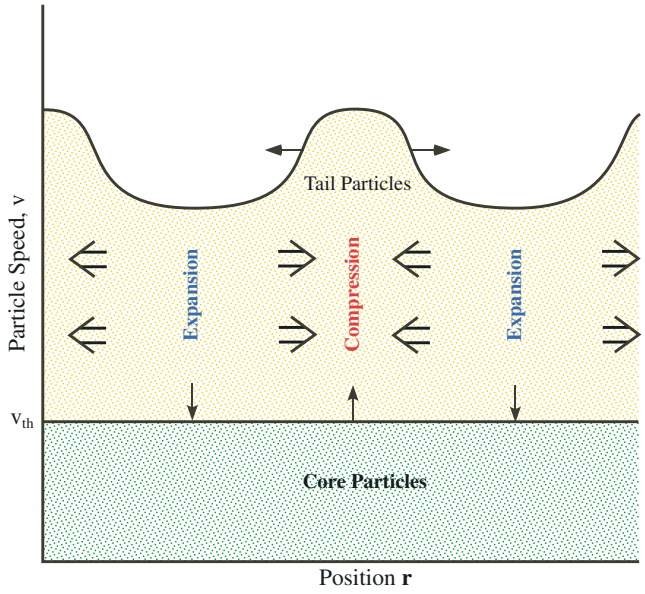

Figure 8. A schematic illustration of the principles underlying the pump acceleration mechanism of Fisk and Gloeckler.

spectrum is also pronounced downstream from shocks, which is also a subsonic region with compression and expansion regions, with a ready source of particles to accelerate—the solar wind that is heated when crossing the shock (section 2.1). The common spectrum is also strongest in the slow solar wind, which tends to have compressive turbulence, as opposed to the fast solar wind from the polar coronal holes, where the turbulence is more Alfvenic (section 2.3).

We can thus assume that a region containing large-scale compressions and expansions is a requirement for the common spectrum, and presumably also a source of particles to accelerate is required. The regions where the common spectrum occurs also do not exhibit strong average spatial gradients. The spatial variations in the average ACR intensity in the heliosheath or in the accelerated particles downstream from shocks are small relative to the scale sizes of the turbulence. The absence of large-scale spatial gradients across the volume where particles are accelerated has the consequence that the volume can be considered to be thermally isolated. The flows across any spatial boundaries are uncorrelated, with the result that particles are being accelerated in the volume, not elsewhere and flowing into the volume, and particles are not being lost from the volume.

3.2. An Illustration of How the Acceleration Mechanism Works

To understand how particles can be accelerated in the conditions described in the previous section, it is useful to consider the illustration in Figure 8. We have a volume of plasma containing compressions and expansions. Particle speed is plotted on the vertical axis and position on the horizontal axis. There are three particle populations in the volume: (a) the thermal plasma, e.g., the thermal solar wind, which contains the mass and is responsible for the random compressions and expansions (not shown in figure), (b) a particle population with speeds greater than the thermal speed of the bulk plasma and less than an upper threshold speed, $v \leq v_{th}$, which is the source particle population. The source particles also undergo random compressions and expansions but are not mobile and do not readily escape by spatial diffusion from a compression/expansion region, e.g., interstellar pickup ions in the solar wind make an ideal source particle population or heated solar wind downstream from shocks. (c) A particle population with speeds above v_{th} that is being accelerated out of the source particle population. The distinction between the source and the accelerated particles is that the accelerated particles can spatially diffuse and escape from a compression or diffuse into an expansion region.

Consider then what happens in the compression shown in the center of Figure 8. The source particles are compressed adiabatically, and energy and particles flow across the threshold boundary at $v = v_{th}$. The accelerated particles are also compressed adiabatically and raised in energy, as noted by the extension in the compression region to higher-particle speeds.

The opposite behavior occurs in the two expansion regions on either side of the compression region. In the expansion regions, particles and energy flow from the accelerated particle population back into the source particle population and the energy of the accelerated particles is reduced. Note the large spatial gradients that result at higher-particle speeds between the compression and the surrounding expansion regions. Accelerated particles are able to spatially diffuse, and so at higher-particle speeds, particles will diffuse in response to these gradients, out of the compression region into the surrounding expansion regions.

Subsequently, the compression region will become an expansion region, and the process will be reversed. Particles and energy will flow back into the source from the accelerated particles. However, since particles have escaped from the compression region by spatial diffusion, there are fewer particles and less energy to return to the source.

If the process of compressions and expansions is repeated sequentially, then the accelerated particles and the energy they contain will systematically increase in time. This is a classic pump mechanism. The combination of adiabatic compressions and expansions, and spatial diffusion of the accelerated particles, will pump particles out of the source population and extend the distribution of the accelerated particles to higher and higher energies.

3.3. The Parker Equation Describes the Behavior of the Accelerated Particles

The appropriate equation that describes the behavior of the accelerated particles is the standard Parker transport equation, which is used in cosmic ray modulation studies. The compression and expansion regions in Figure 8 have large cross-sectional dimensions compared to the gyroradii of the particles that are being accelerated, and thus each is like a small modulation region. The distribution function of the particles being accelerated, $f(\mathbf{r}, n, t)$, thus behaves as

$$\frac{\partial f}{\partial t} + \delta\mathbf{u}\cdot\nabla f = \frac{\nabla\cdot\delta\mathbf{u}}{3} v\frac{\partial f}{\partial v} + \nabla\cdot(\widetilde{\kappa}\cdot\nabla f). \tag{2}$$

Here $\delta\mathbf{u}$ is the convective velocity of the compressions and expansions and $\widetilde{\kappa}$ is the spatial diffusion tensor. Note that implicit in the Parker equation is the assumption that there is a magnetic field that will couple the particle behavior within the compression and expansion regions.

It is important to note that the compression and expansion regions in equation (2) are not random and are correlated with each other. We have a fixed volume in which the acceleration occurs, which requires that each compression region must be surrounded by expansion regions. This is a fundamentally different assumption than assuming that the compressions and expansions are random. The former assumption of correlated expansions/compressions will lead to the pump acceleration mechanism illustrated in Figure 8; the latter assumption of random compressions and expansions will lead to traditional stochastic acceleration.

We can see the role of our assumption of a fixed, thermally isolated volume by integrating equation (2) over all particle speeds above the threshold speed that separates the low-energy source of particles from the accelerated particles, $v \geq v_{\mathrm{th}}$, and over the fixed volume to form an equation for the behavior of the pressure, P, of the accelerated particles. The resulting equation contains divergences of flows of energy, which when integrated over the volume become flows across the spatial boundaries. The system is thermally isolated, in which case the boundary terms become zero, and we find that

$$\int_{\mathrm{vol}} \mathrm{d}(\mathrm{vol})\left[\frac{\partial P}{\partial t} + \delta\mathbf{u}\cdot\nabla P + \frac{5}{3}(\nabla\cdot\delta\mathbf{u})P\right] = -\int_{\mathrm{vol}} \mathrm{d}(\mathrm{vol})\frac{\nabla\cdot\delta\mathbf{u}}{3}\frac{4\pi m}{3} v^5 f|_{v=v_{\mathrm{th}}}, \tag{3}$$

where m is particle mass. The integrand on the left side of equation (3) is the time rate of change of the average pressure in the volume plus the time rate of change of the pressure due to the change in volume in a compression or expansion region. The expression on the right side of equation (3) is the net flow of energy across the threshold boundary due to the compressions and expansions. The total volume of the system is constant. The changes in the pressure due to changes in the volume in a compression or expansion region must thus integrate to zero. Equation (3) then requires that the only source of energy to the average pressure of the accelerated particles is the net flow of energy from the low-energy source of particles, due to the compressions and expansions.

3.4. Why Is the Spectral Index −5?

The acceleration illustrated in Figure 8 is an irreversible process occurring in a thermally isolated volume. A thermally isolated system with an irreversible process will tend to a state of maximum entropy, i.e., the accelerated particles will approach a state of maximum entropy. Yet in a state of maximum entropy, the compressions and expansions continue, and thus each compression and expansion must be isentropic or, equivalently for an ideal gas, adiabatic. At energies below where the rollovers occur in Figure 8, the spatial

gradients are relatively small, in which case spatial diffusion can be ignored, and the behavior of the accelerated particles in this portion of the spectrum, from equation (2), is described by

$$\frac{\partial f}{\partial t} + \delta\mathbf{u}\cdot\nabla f - \frac{\nabla\cdot\delta\mathbf{u}}{3} v\frac{\partial f}{\partial v} = 0. \tag{4}$$

In order for each compression and expansion to be adiabatic (isentropic), the pressure P in the portion of spectrum governed by equation (4) must satisfy the equation for an adiabatic or isentropic compression or expansion:

$$\frac{\partial P}{\partial t} + \delta\mathbf{u}\cdot\nabla P + \frac{5}{3}(\nabla\cdot\delta\mathbf{u})P = 0. \tag{5}$$

If we have a power law spectrum, $f \propto v^{-\alpha}$, then in order for the pressure associated with the power law portion of the spectrum to satisfy equations (4) and (5), α must be 5.

3.5. Deriving an Equation for the Time Evolution of the Common Spectrum

In order to turn the Parker equation (2) into an equation that describes the time evolution of the common spectrum, we take the following steps: Step (1) we divide f into a mean term and a variable term, $f = f_o + \delta f$, but unlike other approaches, we make nonconventional definitions of f_o and δf that will facilitate obtaining our required equation; Step (2) we approximate the spatial diffusion term in equation (1) as a loss/gain term; Step (3), with Steps (1) and (2), we can derive the equation for the time evolution of the common spectrum simply by inspection of equation (2).

1. We define f_o and δf in terms of the spatially averaged pressure P_o and the local deviation in the pressure in a compression or expansion region, δP, or

$$P_o = \frac{4\pi m}{3}\int_{v_{th}}^{\infty} v^4 f_o \mathrm{d}v \quad \text{and} \quad \delta P = \frac{4\pi m}{3}\int_{v_{th}}^{\infty} v^4 \delta f \mathrm{d}v, \tag{6}$$

   where, by definition, $\langle\delta P\rangle = 0$; the angular brackets denote spatial average.

It is important to note the f_o and δf in equation (6) are defined in fundamentally different ways than in traditional stochastic acceleration, as considered, e.g., by *Jokipii and Lee* [2010]. In traditional stochastic acceleration, f_o is defined as the spatial average of f at each particle speed, in which case the spatial average of δf is $\langle\delta f\rangle = 0$. In equation (6), δf is integrated over particle speed to determine the pressure, which in turn averages to zero. Since the spectrum of δf varies between compression and expansion regions, δf as defined in equation (6) clearly does not necessarily average to zero.

2. The diffusion term in equation (2) is difficult to deal with, since it involves local gradients. We can, however, approximate the effects of the diffusion, with a loss/gain term, $\delta f/\tau$, where τ is the characteristic time for escape due to spatial diffusion. Note that in this approximation of spatial diffusion, τ is a quantity that needs to be solved for. The escape time τ depends upon the spatial diffusion coefficient, but it also depends upon the spatial gradients in the variable δf.
3. Then, substituting in $f = f_o + \delta f$, approximating the diffusion term as a loss/gain term, and rearranging terms, equation (2) becomes

$$\begin{aligned}\frac{\partial(f_o+\delta f)}{\partial t} + \delta\mathbf{u}\cdot\nabla(f_o+\delta f) + \frac{5}{3}(\nabla\cdot\delta\mathbf{u})(f_o+\delta f) \\ = \frac{\nabla\cdot\delta\mathbf{u}}{3v^4}\frac{\partial}{\partial v}\left(v^5\delta f\right) + \frac{\nabla\cdot\delta\mathbf{u}}{3v^4}\frac{\partial}{\partial v}\left(v^5 f_o\right) - \frac{\delta f}{\tau}.\end{aligned} \tag{7}$$

We then determine the equation for f_o by inspection by first integrating equation (7) to form an equation for the pressure, and then over volume:

$$\frac{4\pi m}{3}\int_{\mathrm{vol}}\mathrm{d}(\mathrm{vol})\int_{v_{th}}^{\infty} v^4\mathrm{d}v\left[\begin{aligned}\frac{\partial(f_o+\delta f)}{\partial t} + \delta\mathbf{u}\cdot\nabla(f_o+\delta f) + \frac{5}{3}(\nabla\cdot\delta\mathbf{u})(f_o+\delta f) \\ - \frac{\nabla\cdot\delta\mathbf{u}}{3v^4}\frac{\partial}{\partial v}\left(v^5\delta f\right) - \frac{\nabla\cdot\delta\mathbf{u}}{3v^4}\frac{\partial}{\partial v}\left(v^5 f_o\right) + \frac{\delta f}{\tau}\end{aligned}\right] = 0. \tag{8}$$

We then compare equation (8) with equation (3), which states that the only source of energy to the average pressure of the accelerated particles is the net flow of energy from the low-energy source of particles, due to the compressions and expansions. Equivalently f_o, which determines the average pressure, can vary in time only due to the second-order average flow of energy from the low-energy source or

$$\frac{\partial f_o}{\partial t} = \frac{1}{v^4}\frac{\partial}{\partial v}\left(\frac{v^5\langle(\nabla\cdot\delta\mathbf{u})\delta f\rangle}{3}\right). \tag{9}$$

We then subtract equation (9) from equation (8), use the definitions of P_o and δP in equation (6), and rearrange the terms as

$$\begin{aligned}
&\int_{\text{vol}} \mathrm{d(vol)}\left[\frac{\partial(\delta P)}{\partial t} + \delta\mathbf{u}\cdot\nabla(\delta P) + \frac{5}{3}(\nabla\cdot\delta\mathbf{u})(P_o+\delta P)\right] \\
&= \frac{4\pi m}{3}\int_{\text{vol}} \mathrm{d(vol)}\int_{v_{\text{th}}}^{\infty} v^4 \mathrm{d}v\left[-\frac{\nabla\cdot\delta\mathbf{u}}{3v^4}\frac{\partial}{\partial v}\left(v^5 f_o\right) + \frac{\delta f}{\tau}\right] \\
&= \frac{4\pi m}{3}\int_{\text{vol}} \mathrm{d(vol)}\left[-\frac{\nabla\cdot\delta\mathbf{u}}{3}v^5 f_o\big|_{v=v_{\text{th}}} - \int_{v_{\text{th}}}^{\infty} v^4\frac{\delta f}{\tau}\right]\mathrm{d}v.
\end{aligned} \tag{10}$$

Variations with time in the pressure, δP, are the result only of variations in the volume, and since the total volume is constant, and thermally isolated, the left side of equation (10) must integrate to zero or

$$\frac{4\pi m}{3}\int_{\text{vol}} \mathrm{d(vol)}\left[-\frac{\nabla\cdot\delta\mathbf{u}}{3}v^5 f_o\big|_{v=v_{\text{th}}} - \int_{v_{\text{th}}}^{\infty} v^4\frac{\delta f}{\tau}\right]\mathrm{d}v = 0. \tag{11}$$

The first term on the right of equation (11) is the net first-order flow of energy into the accelerated particles due to compressions and expansions. The second term is the net flow of energy into or out of expansion and compression regions due to spatial diffusion.

Consider then the circulation of energy between compression and expansion regions. By definition, each compression region must be surrounded by an expansion region. Energy flows into a compression region from the low-energy source of particles, according to the first term in the integrand of equation (11), and then outward into the surrounding expansion region by spatial diffusion, according to the second term. In the surrounding expansion region, the energy that flows inward by spatial diffusion from the compression region flows outward to the low-energy source. To first order, the energy that flows back to the source in the surrounding expansion region must equal the energy that flows from the source into the compression region. This can be realized only if (to first order) all the energy that flows into the compression region from the source escapes by spatial diffusion into the expansion region, and all the energy that flows into the expansion region by spatial diffusion from the compression region flows back into the source. Thus, using the formulation in the second line of equation (10), for each compression and expansion,

$$\frac{\nabla\cdot\delta\mathbf{u}}{3v^4}\frac{\partial}{\partial v}\left(v^5 f_o\right) = \frac{\delta f}{\tau}. \tag{12}$$

Substituting equation (12) into equation (9), we find the desired equation for f_0:

$$\frac{\partial f_o}{\partial t} = \frac{1}{v^4}\frac{\partial}{\partial v}\left(\frac{\left\langle(\nabla\cdot\delta\mathbf{u})^2\tau\right\rangle}{9}v\frac{\partial}{\partial v}\left(v^5 f_o\right)\right). \tag{13}$$

It is evident that the solution to equation (13) is a spectrum of v^{-5} with some form of rollover at higher speeds, where the location of the rollover in particle speed increases with time, as required. To evaluate the location of the rollover, we need to specify τ, which depends upon the local spatial diffusion coefficient, κ, and the spatial gradients in δf in the rollover regions of the spectrum, which have scale sizes on the order of the scale size of a compression or expansion region, which we take to be λ. It is thus reasonable to take

$$\left\langle(\nabla\cdot\delta\mathbf{u})^2\tau\right\rangle \approx \frac{\delta u^2}{\lambda^2}\frac{\lambda^2}{\kappa} = \frac{\delta u^2}{\kappa}. \tag{14}$$

If we then take the local spatial diffusion coefficient for escape from a compression region to have a standard form of particle speed times a power law in particle rigidity, or $\kappa \propto v^{(1+\alpha)}$, the solution to equation (13) is

$$f_o \propto v^{-5} \exp\left[-\frac{9\kappa}{(1+\alpha)^2 \delta u^2 t}\right]. \tag{15}$$

This is the solution for the acceleration of the energetic particles due compressions and expansions in a thermally isolated volume derived by *Fisk and Gloeckler* [2008, 2012a] and *Fisk et al*. [2010].

Finally, we can use our method of solving by inspection to determine the equation for δf, noting from equations (3) and (10) that first-order changes in δP and thus δf are the result only of volume changes, or

$$\frac{\partial \delta f}{\partial t} + \delta \mathbf{u} \cdot \nabla \delta f + \frac{5}{3}(\nabla \cdot \delta \mathbf{u})(f_o + \delta f) \approx 0. \tag{16}$$

Noting that $\delta f \ll f_o$, equation (16) can be solved to yield

$$\delta f = -\frac{5}{3}\int_{t-\tau}^{t} (\nabla \cdot \delta \mathbf{u}) f_o \mathrm{d}t', \tag{17}$$

where the integration is over the past time history as particles are convected with $\delta \mathbf{u}$. We perform the integration only starting at $t - \tau$, i.e., only for a time interval during which the particles have not escaped by local spatial diffusion.

Equation (17) is valid in the -5 portion of the spectrum since here τ is longer than the coherence time of a compression or expansion. In the -5 portion of the spectrum particles undergo compressions and expansions, without escape within a compression time, as described in equation (17). Note that in this region of the spectrum, the spatial average of δf is $\langle \delta f \rangle = 0$.

In the rollover region of the spectrum, τ is short compared to the coherence time of a compression region, and equation (12) determines δf. There is a balance between the flow of energy from the core and escape by spatial diffusion. Substituting equation (15) into equation (12), we find that

$$\delta f = \frac{\tau \nabla \cdot \delta \mathbf{u}}{3v^4} \frac{\partial}{\partial v}\left(v^5 f_o\right) = \frac{3(\nabla \cdot \delta \mathbf{u})}{(1+\alpha)^2}\left(\frac{\kappa}{\delta u^2 t}\right) \tau f_o. \tag{18}$$

In the rollover region the fluctuations are also proportional to $\nabla \cdot \delta \mathbf{u}$, as in the -5 portion of the spectrum, as seen in equation (18), but are intrinsically larger since $\kappa/\delta u^2 t > 1$. However, the particles escape within a compression or expansion time, or $(\nabla \cdot \delta \mathbf{u})\tau < 1$, with the result that the fluctuation δf, relative to f_o, is smaller in the rollover region than in the -5 portion of the spectrum.

Note, however, if we spatially average equation (16) and substitute in equation (12), we find that

$$\frac{\partial \langle \delta f \rangle}{\partial t} = -\frac{2}{3}\langle (\nabla \cdot \delta \mathbf{u}) \delta f \rangle = -\frac{2}{9}\left\langle (\nabla \cdot \delta \mathbf{u})^2 \tau \right\rangle \frac{1}{v^4}\frac{\partial}{\partial v}\left(v^5 f_o\right). \tag{19}$$

Thus, in the rollover region of the spectrum, $\langle \delta f \rangle \neq 0$, unlike in the -5 portion of the spectrum.

3.6. Comparing the Solutions for the Time Evolution of the Common Spectrum With Observations

Observations of the distribution functions of the accelerated particles are usually spatial averages, where the mean distribution at each particle speed is determined, and deviations from the mean at each particle speed are assumed to average to zero. As is described in equation (6), we did not define f_o and δf with the expectation that $\langle \delta f \rangle$ must be zero. However, as we discussed in the previous section, our solution for f_o is a valid description of the observed mean distribution function of accelerated particles at all particle speeds. In the -5 portion of the spectrum there are fluctuations, δf, that depend upon the local value of $\nabla \cdot \delta \mathbf{u}$. They have the same -5 spectrum, and average to zero, as can be seen in equation (17). In the rollover region of the spectrum the fluctuations δf do not have the same spectrum as f_o, as can be seen in equation (12), and do not average to zero, as in equation (19). The average of these fluctuations, however, is small compared to f_o, as can be seen in equation (18), and does not affect the comparison of f_o with observations.

3.7. Why Is the Pump Acceleration the Dominant Acceleration Mechanism?

We should expect that the pump acceleration mechanism illustrated in Figure 8 and described by equations (13) and (15) dominates over any second-order stochastic acceleration process. The pump acceleration includes a first-order acceleration, as can be seen in the schematic, Figure 8. Particles escape from a compression region into an expansion region only after the expansion region has undergone most of its expansion; this is when the spatial gradients are the strongest. Thus, in the cyclic process, particles do not gain and lose an equal amount of energy, as would occur if the particles undergo a stochastic diffusion in velocity space. Rather, the particles gain more energy in a compression region than they lose in the expansion regions into which they escape, resulting in a first-order acceleration.

We can see the first-order acceleration by rewriting the basic equation that describes the pump acceleration, equation (13), as

$$\frac{\partial}{\partial t}\left(v^5 f_o\right)+\frac{\left\langle(\nabla\cdot\delta\mathbf{u})^2\tau\right\rangle v}{3}\frac{\partial}{\partial v}\left(v^5 f_o\right)=\frac{1}{v^2}\frac{\partial}{\partial v}\left(v^4\frac{\left\langle(\nabla\cdot\delta\mathbf{u})^2\tau\right\rangle}{9}\frac{\partial}{\partial v}\left(v^5 f_o\right)\right). \tag{20}$$

Recall that the solutions to the governing equation of the pump acceleration are proportional to v^{-5}. Thus, the quantity $v^5 f_o$ marks where f_o deviates from v^{-5}, i.e., it marks where the rollover in the spectrum occurs. The term on the right side of equation (20) is in the form of a traditional stochastic diffusion. The location of the rollover thus diffuses to higher-particle speeds. The first-order acceleration of the location of the rollover is contained in the second term on the left of equation (20); the first-order acceleration is

$$\frac{\mathrm{d}v}{\mathrm{d}t}=\frac{\left\langle(\nabla\cdot\delta\mathbf{u})^2\tau\right\rangle v}{3}. \tag{21}$$

Thus, if there is a sufficient source particle population present on which the pump acceleration can act, the pump acceleration process will be the dominate determinant of the spectrum of the accelerated particles and yield the $f_o\propto v^{-5}$ spectra that are most commonly observed.

We should also expect, as is discussed in section 2, that the pump acceleration mechanism operating in the downstream region dominates over diffusive shock acceleration (see *Fisk and Gloeckler* [2012a] for a detailed discussion of the relative importance of pump acceleration and diffusive shock acceleration). Particles are accelerated in standard diffusive shock acceleration by experiencing multiple times the strong compression that occurs at the shock front. In that sense, the compression at the shock front is just one of many compressions; other compressions used by the pump acceleration mechanism occur throughout the downstream region. In fact, the compression at the shock front may not be particularly effective. The extent to which particles are accelerated depends upon the time spent in the compression. Shocks are at only one location, whereas the compressions downstream, albeit weaker than the compression at the shock, occur in a much larger volume.

3.8. Some Subtleties Associated With the Solutions for the Pump Acceleration

Finally, we discuss some of the subtleties associated with the derivation of the governing equation for pump acceleration, and the solution to this equation, which appear to have confused some researchers considering this problem.

Jokipii and Lee [2010] argue that density is not properly conserved in equation (9). They integrate equation (9) over all tail particle speeds to find an equation for the time rate of change of the density n_o associated with f_o.

$$\frac{\mathrm{d}n_0}{\mathrm{d}t}=-\frac{4\pi v^3}{3}\langle\delta f\nabla\cdot\delta\boldsymbol{u}\rangle|_{v_{\mathrm{th}}}+\frac{8\pi}{3}\int_{v_{\mathrm{th}}}^{\infty}v^2\mathrm{d}v\langle\delta f\nabla\cdot\delta\boldsymbol{u}\rangle. \tag{22}$$

The first term on the right represents a flow of particles across the threshold boundary from the source particle population, and then *Jokipii and Lee* [2010] state that the second term on the right is a spurious source term that appears to be creating particles.

The actual requirement for the conservation of density is not that the density n_o is conserved, but rather that the total average density is conserved, which is determined by $f_o + \langle \delta f \rangle$. If we combine equations (19) and (9), we find

$$\frac{\partial f_o}{\partial t} + \frac{\partial \langle \delta f \rangle}{\partial t} = \frac{1}{v^4}\frac{\partial}{\partial v}\left(\frac{v^5 \langle (\nabla \cdot \delta \mathbf{u}) \delta f \rangle}{3}\right) - \frac{2}{3}\langle (\nabla \cdot \delta \mathbf{u}) \delta f \rangle = \frac{1}{v^2}\frac{\partial}{\partial v}\left(\frac{v^3 \langle (\nabla \cdot \delta \mathbf{u}) \delta f \rangle}{3}\right), \tag{23}$$

which when integrated to form the density demonstrates that all accelerated particles originate in the source particle population. There are no spurious source terms. The extra contribution to the density results as follows: there is a balance between energy flowing into and out of the source population, and energy flowing outward and inward by spatial diffusion. However, the energy flowing in and out of the source is carried by low-speed particles, whereas the energy flowing in and out by spatial diffusion is carried by higher-speed particles. Thus, although the energy flows balance, the particle flows do not, yielding an apparent particle source.

There has also been some confusion about the thermodynamics of the pump acceleration process. The basic premise of the pump acceleration mechanism is that there is interplay between acceleration in a compression region and escape by spatial diffusion, versus deceleration in an expansion region and inflow by spatial diffusion. This interplay pumps particles out of a source particle population under circumstances in which no net work is being done on the accelerated particles when averaged over multiple compressions and expansions. The source of energy for the accelerated tail is the energy in the source particles. It might seem then that the pump mechanism is thermodynamically impossible. Particles are being accelerated when no work is being done on them. Energy is flowing from the colder source into the hotter tail.

Consider, however, the following illustrative example. Suppose you have a fixed, thermally isolated volume that contains a gas that is undergoing particle-particle collisions. Suppose also that initially the distribution of the gas is not Maxwellian in that there are too few high-speed particles to be a Maxwellian distribution. In time, the distribution of the gas will evolve into a Maxwellian distribution, which is the state of maximum entropy. The particle-particle collisions will accelerate particles to the high speeds required to satisfy a Maxwellian distribution. Since these are particle-particle collisions, the total energy of the gas is unchanged in the process of accelerating the particles to high speeds. This is thus an example of an irreversible process that transfers particles and energy from a colder portion of the distribution to a hotter high-speed portion, while maintaining the overall thermodynamic constraints that the total energy and density are constants.

The irreversible transfer of energy from the colder core particles to the hotter tail particles for the purpose of maximizing entropy also occurs in the pump acceleration process. We have a fixed volume, thermally isolated system, in which there are not particle-particle collisions, but rather organized compressions and expansions of the gas. There is an embedded magnetic field whose sole purpose is to couple the behavior of particles at all speeds in compression and expansion regions. The compressions and expansions are simply volume changes of the gas, and since the overall volume is constant there is no net work done by the compressions and expansions when summed over the volume. When we add spatial diffusion at tail particle speeds, we find that there is an irreversible flow of particles and energy from the core into the tail, and an irreversible expansion of the tail particles in velocity space (i.e., an acceleration). The pump process thus increases the entropy of our system.

A thermally isolated, constant volume system conserves particles and energy. The evolution of the system is determined by the behavior of the entropy. Allowable evolutions must increase the entropy until the entropy is a maximum, at which point the system can be said to be in equilibrium. The pump acceleration mechanism operates in a thermally isolated, constant volume system; it conserves the total energy and number of particles; and it increases the entropy. It is an allowable evolution of the system, and it will form a tail on the particle distribution function at high-particle speeds.

4. Concluding Remarks

In this paper we have presented relevant observations of and a theoretical explanation for the common spectrum: a distribution function that is a power law with spectral index of −5, with an exponential rollover at higher-particle speeds; or equivalently, a differential intensity spectrum that is a power law with spectral index of −1.5 and an exponential rollover at higher energies. We have cited those observations that are most

revealing of the conditions in which the common spectrum occurs, and we have presented our most detailed and thorough description of how a pump acceleration process operates and yields the time evolution of the common spectrum. We have attempted to deal with all the subtleties and concerns that have been raised concerning the pump acceleration process.

Since the initial introduction of the pump acceleration process [*Fisk and Gloeckler*, 2008], it has been applied with success to the acceleration of ACRs in the heliosheath [*Fisk and Gloeckler*, 2009], to the acceleration of particles downstream of shocks [*Fisk and Gloeckler*, 2012a], and to the acceleration of galactic cosmic rays in the interstellar medium [*Fisk and Gloeckler*, 2012b]. There is also ongoing work on the influence of the pump acceleration mechanism on the source particle population from which more energetic particles are accelerated, as well as the application of pump acceleration to various solar phenomena, e.g., impulsive solar energetic particle events, large-scale solar particle events caused by coronal mass ejections, and seed particles in the solar corona.

It is important to emphasize that the common spectrum is a real, observed phenomenon in the heliosphere, observed at shocks in the inner heliosphere, and in the ACRs throughout the heliosheath. We encourage every theorist and observer who is currently studying particle acceleration in the heliosphere or in other astrophysical settings, by using diffusive shock acceleration or some form of traditional stochastic acceleration, to consider whether the pump acceleration mechanism that yields the common spectrum might provide a better description of the acceleration they are studying. We should all recognize that there are new phenomena in heliospheric physics, which when understood will prove the relevance of our discipline to astrophysics.

Acknowledgments

This work was supported in part by NASA grants NNX10AF23G, NNX13AE056, and NNX11AP01G and by NSF grant AGS-1344835. In compliance with AGU Data Policy, all data used in this paper are available from the references cited.

Yuming Wang thanks the reviewers for their assistance in evaluating this paper.

References

Antecki, T., R. Schlickeiser, and M. Zhang (2013), Stochastic acceleration of suprathermal particles under pressure balance conditions, *Astrophys. J.*, *764*, doi:10.1088/0004-637X/764/1/89.

Bykov, A. M. (2001), Particle acceleration and nonthermal phenomena in superbubbles, *Space Sci. Rev.*, *99*(1/4), 317–326.

Decker, R. B., E. C. Roelof, S. M. Krimigis, and M. E. Hill (2006), Low-energy ions near the termination shock, in *Physics of the Inner Heliosheath*, AIP Conference Proceedings, vol. 858, pp. 73–78, AIP, Melville.

Drake, J. F., M. Swisdak, and R. Fermo (2013), The power-law spectra of energetic particles during multi-island magnetic reconnection, *Astrophys. J. Lett.*, *763*, doi:10.1088/2041-8205/763/1/L5.

Fisk, L. A., and G. Gloeckler (2007), Thermodynamic constraints on stochastic acceleration in compressional turbulence, *Proc. Natl. Acad. Sci. U.S.A.*, *104*, 5749–5754.

Fisk, L. A., and G. Gloeckler (2008), Acceleration of suprathermal tails in the solar wind, *Astrophys. J.*, *686*, 1466–1473.

Fisk, L. A., and G. Gloeckler (2009), The acceleration of anomalous cosmic rays by stochastic acceleration in the heliosheath, *Adv. Space Res.*, *43*, 1471–1478.

Fisk, L. A., and G. Gloeckler (2012a), Particle acceleration in the heliosphere: Implications for astrophysics, *Space Sci. Rev.*, *173*, 433–458.

Fisk, L. A., and G. Gloeckler (2012b), Acceleration of galactic cosmic rays in the interstellar medium, *Astrophys. J.*, *744*, doi:10.1088/0004-637X/744/2/127.

Fisk, L. A., and G. Gloeckler (2013), The global configuration of the heliosheath inferred from recent Voyager 1 observations, *Astrophys. J.*, *776*, doi:10.1088/0004-637X/776/2/79.

Fisk, L. A., and G. Gloeckler (2014), On whether or not Voyager 1 has crossed the heliopause, *Astrophys. J.*, *789*, doi:10.1088/0004-637X/789/1/41.

Fisk, L. A., G. Gloeckler, and N. A. Schwadron (2010), On theories for stochastic acceleration in the solar wind, *Astrophys. J.*, *720*, 533–540.

Gloeckler, G., and L. A. Fisk (2010), Proton velocity distributions in the inner heliosheath derived from energetic hydrogen atoms measured with Cassini and IBEX, in *Pickup Ions Throughout the Heliosphere and Beyond*, *AIP Conf. Proc.*, vol. *1302*, edited by J. A. le Roux et al., p. 110, AIP, Melville.

Gloeckler, G., and L. A. Fisk (2014), A test for whether or not Voyager 1 has crossed the heliopause, *Geophys. Res. Lett.*, *41*, 5325–5330, doi:10.1002/2014GL060781.

Gloeckler, G., et al. (1992), The Solar Wind Ion Composition Spectrometer, *Astron. Astrophys. Suppl. Ser.*, *92*, 267–289.

Gloeckler, G., L. A. Fisk, G. M. Mason, and M. E. Hill (2008), Formation of power law tail with spectral index −5 inside and beyond the heliosphere, in *Particle Acceleration and Transport in the Heliosheath and Beyond*, *AIP Conf. Proc.*, vol. 1039, pp. 367–374, AIP, Melville.

Gosling, J. T. (2012), Magnetic reconnection in the solar wind, *Space Sci. Rev.*, *172*, 187–200.

Jokipii, J. R., and M. A. Lee (2010), Compression acceleration in astrophysical plasmas and the production of f(v) proportion to v^{-5} spectra, *Astrophys. J.*, *713*, 475–483.

Krimigis, S. M., C. O. Bostrom, T. P. Armstrong, W. I. Axford, C. Y. Fan, G. Gloeckler, and L. J. Lanzerotti (1997), The Low Energy Charged Particle/LECP/experiment on the Voyager spacecraft, *Space Sci. Rev.*, *21*, 329–354.

Krimigis, S. M., et al. (2013), Search for the exit: Voyager 1 at heliosphere's border with the galaxy, *Science*, *341*, 144–147.

Lario, D., Q. Hu, G. C. Ho, R. B. Decker, E. C. Roelof, and C. W. Smith (2005), Statistical properties of fast forward transient interplanetary shocks and associated energetic particle events: ACE observations, in *Proc. Solar Wind 11–SOHO 16 "Connecting Sun and Heliosphere"*, ESA SP-592, edited by B. Fleck, T. H. Zurbuchen, and H. Lacoste, pp. 81–86, Noordwijk, Netherlands.

Livadiotis, G., and D. J. McComas (2009), Beyond kappa distributions: Exploiting Tsallis statistical mechanics in space plasmas, *J. Geophys. Res.*, *114*, A11105, doi:10.1029/2009JA014352.

Livadiotis, G., and D. J. McComas (2011), Invariant kappa distribution in space plasmas out of equilibrium, *Astrophys. J.*, *741*, doi:10.1088/0004-637X/741/2/88.

Livadiotis, G., and D. J. McComas (2012), Non-equilibrium thermodynamics processes: Space plasmas and the inner heliosheath, *Astrophys. J.*, *749*, doi:10.1088/0004-637X/749/1/11.

Livadiotis, G., and D. J. McComas (2013), Understanding kappa-distributions: A toolbox for space science and applications, *Space Sci. Rev.*, *175*, 183–214.

Schwadron, N. A., and D. J. McComas (2006), Modulation of anomalous and galactic cosmic rays beyond the termination shock, *Geophys. Res. Lett.*, *34*, L14105, doi:10.1029/2007GL029847.

Schwadron, N. A., M. A. Dayeh, M. Desai, H. Fahr, J. R. Jokipii, and M. A. Lee (2010), Superposition of stochastic processes and the resulting particle distributions, *Astrophys. J.*, *713*, 1386–1392.

Stone, E. C., R. E. Vogt, F. B. McDonald, B. J. Teegarden, J. H. Trainor, J. R. Jokipii, and W. R. Webber (1977), Cosmic ray investigation for the Voyager missions: Energetic particle studies in the outer heliosphere—And beyond, *Space Sci. Rev.*, *21*, 355–376.

Stone, E. C., A. C. Cummings, F. B. McDonald, B. C. Heikkila, N. Lal, and W. R. Webber (2013), Voyager 1 observes low-energy galactic cosmic rays in a region depleted of heliospheric ions, *Science*, *341*, 150–153.

Zhang, M., and M. A. Lee (2013), Stochastic acceleration of energetic particles in the heliosphere, *Space Sci. Rev.*, *176*, 133–146.